

Vacancy-vacancy interaction and oxygen diffusion in stabilized cubic ZrO_2 from first principlesF. Pietrucci,^{1,2} M. Bernasconi,¹ A. Laio,² and M. Parrinello³¹*Dipartimento di Scienza dei Materiali, Università di Milano-Bicocca, Via R. Cozzi 53, I-20125, Milano, Italy*²*International School for Advanced Studies (SISSA), Via Beirut 2-4, I-34014 Trieste, Italy*³*Computational Science, Department of Chemistry and Applied Biosciences, ETH Zurich, USI Campus, Via Giuseppe Buffi 13, 6900 Lugano, Switzerland*

(Received 5 June 2008; revised manuscript received 15 August 2008; published 10 September 2008)

Based on *ab initio* and classical molecular-dynamics simulations, we investigate the role of vacancy-vacancy interaction in oxygen conductivity of yttria-stabilized and scandia-stabilized cubic zirconia. It turns out that a sizable fraction of possible configurations of vacancies are local unstable, although the vacancies are at least third nearest neighbors each other. Investigation of oxygen migration pathways by *ab initio* metadynamics simulations show the occurrence of multiple-vacancy concerted jumps in correspondence of an unstable arrival state for a single vacancy jump. Furthermore, in the case of single vacancy jump, we have observed a strong dependence of the activation barrier on the position of the other vacancies, similar in strength to the dependence of the activation energy on the presence of nearest-neighbors yttrium ions, customarily assumed to constitute a blocking site for vacancy migration. Our results point to the need of improving existing models for oxygen diffusion in stabilized zirconia by including vacancy-vacancy interactions.

DOI: 10.1103/PhysRevB.78.094301

PACS number(s): 66.30.hd, 66.30.Dn, 71.15.Pd

I. INTRODUCTION

Zirconia (ZrO_2), stabilized in the cubic fluorite phase by the addition of substitutional aliovalent metals (e.g., Y^{3+} , Sc^{3+} , Ca^{2+}), is a fast oxygen conductor. In particular, yttria- (Y_2O_3) stabilized zirconia (YSZ) is the most common solid electrolyte used in solid oxide fuel cells and oxygen sensors.¹ Ionic conductivity is provided by mobile oxygen vacancies introduced by the aliovalent dopant atoms for charge compensation. Although the number of vacancies increases monotonically with dopant concentration, the ionic conductivity of doped zirconia always exhibits a maximum for some critical dopant composition with significant decrease at higher dopant contents. The mechanism responsible for this nonmonotonic behavior is still debated, despite decades of intensive investigation.² The dependence of conductivity on dopant concentration has been customarily ascribed to yttrium-vacancy interactions, involving some kind of binding between the two defects which would inhibit diffusion at high dopant contents.³⁻⁶ Theoretical modeling^{4,7} and extended x-ray absorption fine structure (EXAFS) (Refs. 8-11) and nuclear magnetic resonance (NMR) experiments¹² have shown for instance that yttrium ions are preferentially second-nearest neighbor to oxygen vacancies. Computer simulations based on classical molecular dynamics¹³ have suggested instead that the nonmonotonic behavior of the conductivity might be due to the increase at higher dopant content of blocking sites for diffusion in the form of pairs of nearest-neighbor dopant atoms (YY pair in YSZ for instance). Monte Carlo simulations^{14,15} on simple lattice models have shown that the presence of blocking sites seems indeed necessary to reproduce the experimental dependence of conductivity on dopant concentration. More recently, *ab initio* calculations have confirmed this scenario showing that oxygen migration out of tetrahedral sites across a Y-Zr or Y-Y edge (or Sc-Sc edge in Scandia-stabilized zirconia, ScSZ) requires larger activation energies than migrations

across a Zr-Zr edge.¹⁶⁻¹⁸ An increase in the concentration of blocking sites due to dopant migration has also been proposed as a possible source of electrolyte aging.¹⁹ Kinetic Monte Carlo models based on *ab initio* activation energies have been developed to test the blocking sites scenario over long time scales, reaching qualitative agreement with experiments.¹⁶⁻¹⁸ In all these models vacancy-vacancy interactions have been neglected, which, however, might be a too severe assumption also in view of the fact that quantitative agreement with experimental data on conductivity has not been achieved yet. A possible role of vacancy-vacancy interaction in diffusion is suggested for instance by the formation of divacancy complexes, as it can be inferred from diffuse neutron scattering data.²⁰ It has been proposed that vacancies can be associated in pairs along the $\langle 111 \rangle$ directions, which, at high vacancy (dopant) concentration in YSZ, undergo a clustering into the $\text{Zr}_3\text{Y}_4\text{O}_{12}$ -ordered compound. Clusters of this crystalline compound would not contribute to the conductivity due to a low mobility of oxygen vacancies. Theoretical support to the ordering of vacancies in YSZ has been provided by *ab initio* calculations, although on small-size systems.²¹⁻²³ A sixfold coordinated cation at the center of a vacancy pair along $\langle 111 \rangle$ has been also proposed as the defect responsible for the prominent trigonal (*T* center) signal in electron paramagnetic resonance (EPR) spectra and for the optical absorption band at 370 nm of samples chemically reduced or exposed to ionizing radiations.^{24,25} In a previous²⁶ *ab initio* study of divacancy complexes in YSZ we found that several configurations of yttrium ions and vacancies were not even metastable. In fact, the system often transforms spontaneously by displacing one or two vacancies during steepest-descent optimization of the geometry. This result was rather unexpected, considering that the unstable configurations did not show any manifestly unphysical feature: the vacancies were always at least third nearest neighbor among each other and next nearest neighbors to Y ions. Since ionic diffusion can be viewed as a sequence of transitions between the set of locally stable configurations, the exclusion of a sizable frac-

tion of structures might lead to a significantly reduced conductivity.

In this work we investigate further the role of vacancy-vacancy interaction by addressing several issues within *ab initio* calculations. First, we have optimized the geometry of a large number of structures with different distributions of defects (vacancies and Y) to assess the local stability of different configurations. Second, we have explored the mechanism of vacancy diffusion considering simple and concerted jumps within both metadynamics and constrained molecular-dynamics simulations in YSZ and ScYZ.

II. STABILITY OF DEFECT CONFIGURATIONS

We have modeled YSZ with a cubic supercell containing 93 atoms and three oxygen vacancies at composition 10.3 mol% of yttria. The simulation cell corresponds to $2 \times 2 \times 2$ conventional cubic cells (61 O, 6 Y, and 26 Zr atoms). Simulations have been performed within density functional theory in the local density approximation (LDA).²⁷ Brillouin-zone integration has been restricted to the Γ point. Ultrasoft²⁸ and norm-conserving²⁹ pseudopotentials for oxygen and metal ions, respectively, and plane-wave expansion of Kohn-Sham orbitals up to a kinetic cutoff of 30 Ry have been used for geometry optimizations as implemented in the CPMD code.³⁰ Semicore s, p states have been included as valence electrons for Y, Sc, and Zr. The experimental lattice parameters for YSZ ($a=10.22$ Å) (Ref. 31) and ScSZ ($a=10.18$ Å) (Ref. 32) have been used. This framework has been validated in our previous works on bulk and surface properties YSZ and resulted in good agreement with experimental data for both structural and electronic properties.^{7,26,33}

136 different configurations of this system are generated in the following manner. We have first selected eight stable configurations of Y and vacancies. In these configurations, the vacancies are at least third nearest neighbors each other. Yttrium ions are positioned according to three different distributions (Y1, Y2, Y3, see below), and all vacancies have at least two Y at the next-nearest-neighbor positions. In six out of the eight initial configurations, vacancies are at least second nearest neighbor to the Y atoms; while in the remaining two configurations vacancies are also nearest neighbors to Y, namely

- (i) Yttrium distribution Y1: four vacancies configurations. In one configuration Y is nn to one vacancy.
- (ii) Yttrium distribution Y2: two vacancies configurations. In one configuration two vacancies have one Y nearest neighbor.
- (iii) Yttrium distribution Y3: two vacancies configurations.

From these eight structures, we have then generated 136 configurations by attempting the jump of one vacancy to a nearest position along $\langle 100 \rangle$ (three vacancies/cell and six $\langle 100 \rangle$ jump directions, the number of distinct configurations is less than $8 \times 6 \times 3 = 144$ because few configurations are identical). Such trial jumps are realized by putting the vacancy in the arrival state with all the atoms initially in ideal fluorite positions. Then, the atoms are moved according to the average relaxation pattern around

TABLE I. Classification of different configurations of vacancies corresponding to attempted jumps of a single vacancy in a small cell (93-atoms and three vacancies) investigated *ab initio*. The YSZ models contain 10.3 mol% of yttria. The four types of jump are described in the text and in Fig. 1.

<i>ab initio</i>	
total jumps	136
locally stable	49%
locally unstable	51%
type 1 (allowed single)	49%
type 2 (reflected single)	25%
type 3 (long single)	13%
type 4 (concerted)	14%

an isolated vacancy found in our previous work⁷ and in experiments,²⁰ namely oxygen atoms approach the neighboring vacancy along $\langle 100 \rangle$ by 0.3 Å while metal atoms move away from the vacancy along $\langle 111 \rangle$ by 0.2 Å. This partially relaxed atomic configuration is taken as the starting point of *ab initio* geometry optimization, accomplished by Car-Parrinello simulated annealing³⁴ and Broyden-Fletcher-Goldfarb-Shanno relaxation.³⁵ On the accuracy of density-functional theory generalized gradient approximation (DFT-GGA) framework in the description of defects in oxides see Ref. 36.

The results of the geometry optimizations are reported in Table I: 49% of the defect configurations are (locally) stable and 51% are locally unstable. This means that half of the conceivable jumps of a single vacancy to a nearest site are not possible because of the lack of a locally stable arrival state. Referring to the three vacancies in the simulation cell as V_1 , V_2 , and V_3 , we have observed four possible fates for the attempted jump of V_1 from the initial lattice site A to the nearest-neighbor site B (Fig. 1):

- (1) V_1 remains in B (allowed single jump)
- (2) V_1 returns back to A (reflected jump-attempt)
- (3) V_1 spontaneously jumps to a lattice site C different from both A and B (long jump)
- (4) V_1 remains in B but V_2 and/or V_3 spontaneously jumps to a new position and remains there (concerted multiple jump).

It is worth emphasizing that the very existence of concerted two- or three-vacancy jumps (case 4) implies that the local stability of configurations depends on the relative position of vacancies, i.e., for a given yttrium configuration, a vacancy can or cannot occupy a given lattice site depending on the position of the surrounding vacancies.

One may wonder whether finite-size effects, due to the small size of our simulation cell, would be responsible for the observed local instability. Since enlarging the simulation cell above 100-atom size is too expensive in *ab initio* calculations, we have explored whether a classical interatomic potential for YSZ would reproduce the instabilities identified from first principles. To this aim we have first repeated the calculations outlined above on the 93-atom supercell with the two-body potential of Ref. 37, which had been validated by molecular-dynamics simulations of the ionic conductivity

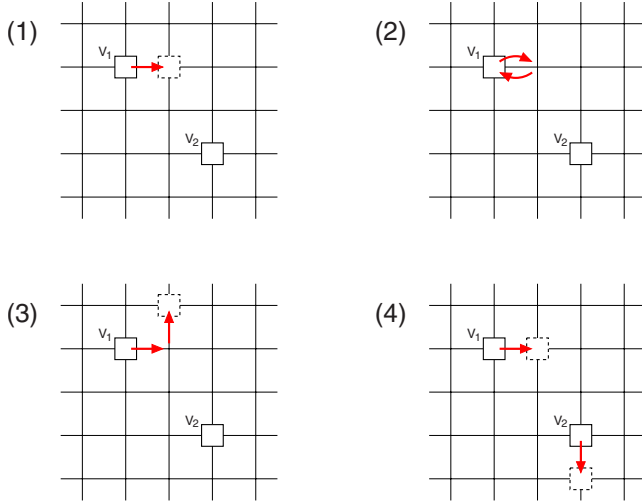


FIG. 1. (Color online) Sketch of the four possible outcomes of the attempted jump of a vacancy (V_1) to a nearest-neighbor position in the presence of a second vacancy (V_2). The square lattice represents the simple cubic oxygen sublattice in YSZ, the drawing is two dimensional for simplicity. Starting from a relaxed model of YSZ, a new model is generated by moving V_1 to the nearest-neighbor site. Depending on the yttrium and vacancy configuration four possible events have been observed during geometry optimization. (1) V_1 remains in the new position (allowed single jump), (2) V_1 returns back to the original position (reflected jump-attempt), (3) V_1 spontaneously jumps to another position different from the original one (long jump), or (4) V_1 remains in the new position but at the same time another vacancy (V_2) spontaneously jumps to a new position (concerted multiple jump).

at high temperature and by comparison with diffuse neutron scattering³⁸ and thermal conductivity data.³⁹ The interatomic potential between two atoms of species i and j at distance r is the sum of long-range pointlike Coulomb interactions plus a short-range repulsion and a van der Waals attraction as $V_{ij} = \frac{Z_i Z_j}{r} + A_{ij} \exp(-r/\rho_{ij}) - \frac{C_{ij}}{r^6}$.³⁷ We started from 116 independent defect configurations, for a total of $116 \times 3 \times 6 = 2088$ attempted single vacancy jumps. The lattice parameter is the same as in the *ab initio* simulations. The results in Table II show that the percentage of unstable configurations (77%) is even larger in the classical models than in the *ab initio* ones, although often a configuration stable in the classical model is unstable in the *ab initio* calculation and vice-versa. This suggests that the stable/unstable character of a distribution of defects relies on a fine balance between Coulombic forces and short-range “elastic” interactions due to the complex (and large) relaxation patterns around the defects.

Within the classical model, we have checked for possible finite-size effects by considering a supercell eight times larger ($93 \times 8 = 744$ atoms and $3 \times 8 = 24$ vacancies, still corresponding to 10.3 mol% of yttria). As before, starting from six independent locally stable defect configurations, all possible jumps of a single vacancy are attempted for each vacancy, and the $24 \times 6 \times 6 = 862$ arrival states are relaxed.

The results, reported in Table II, show that the number of unstable defect configurations is even larger in the 744 atoms cell. Most of the concerted jumps (62%) resulting from lo-

TABLE II. Classification of different configurations of vacancies corresponding to attempted jumps of a single vacancy from classical simulations. Small (93-atoms and three vacancies) and large (744 atoms) cells have been optimized with the classical two-body potential of Ref. 37 (see text). The YSZ models contain 10.3 mol% of yttria. The four types of jump are described in the text and in Fig. 1.

Classical simulations	93 atoms	744 atoms
total jumps	2088	862
locally stable	23%	7%
locally unstable	77%	93%
type 1 (allowed single)	23%	7%
type 2 (reflected single)	12%	37%
type 3 (long single)	35%	11%
type 4 (concerted)	30%	45%

cally unstable arrival states (type 4 in Fig. 1) are double, i.e., two vacancies jump in a concerted way. These results suggest that the destabilization of some configurations of defects is not an artifact of the artificial periodic arrays of vacancies introduced by the boundary conditions on a small cell. Moreover, the larger percentage of unstable configurations in the larger cell suggests that the instabilities are perhaps due to short/medium-range interaction between vacancies. Since we have generated a supercell with a homogeneous distribution of vacancies, the instabilities of, let us say, three vacancies in a 93-atom subcell would turn unstable a large number of configurations of the large cell made of $2 \times 2 \times 2$ 93-atom subcells.

We have attempted to correlate the stable/unstable character of a configuration to geometric parameters, like the distances between vacancies and between yttrium and vacancies, or to energetic parameters, like the variation of total potential energy or electrostatic energy upon relaxation. Unfortunately, we did not find any correlation which could aid to predict whether a given defect configuration is locally stable, but for the trivial situations in which vacancies are nearest neighbors to other vacancies or to several yttrium ions. Once more, the stability of a defects configuration seems to be dictated by the complex and nonadditive⁷ relaxation patterns around vacancies.

III. TRANSITION MECHANISM BETWEEN TWO STABLE STATES

The concerted jumps discussed in the previous sections have been observed during geometry optimization of unstable defects configurations. We may wonder whether concerted jumps might occur also dynamically during a finite-temperature diffusion process. To explore diffusion events promoted by vacancy-vacancy interactions one can perform finite-temperature molecular-dynamics simulations, which allow predicting unforeseen arrival states. In order to observe thermally activated oxygen jumps in the short span of an *ab initio* molecular-dynamics run, it would be necessary to increase the temperature above 1000 K. However, at high tem-

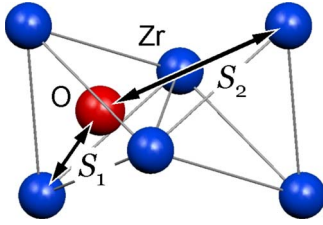


FIG. 2. (Color online) Reaction coordinates in metadynamics simulation of vacancy diffusion: S_1 and S_2 are the Zr-O distances between the diffusing oxygen and a Zr ion in the starting or arrival tetrahedral cage, respectively.

perature it might be difficult to discriminate between concerted multiple jumps and the nearly simultaneous occurrence of several uncorrelated single events. In order to circumvent this limitation, we have performed room-temperature simulations adopting the metadynamics technique, which allows observing rare events with activation barriers much larger than the thermal energy.^{40–42} The method is based on a coarse-grained, non-Markovian dynamics in the manifold spanned by few reaction coordinates biased by a history-dependent potential, which drives the system toward the lowest saddle point. The main assumption is that the reaction path could be described on the manifold of few collective coordinates $S_\alpha(\{\mathbf{R}_I\})$, function of the ionic coordinates \mathbf{R}_I . Following the scheme of Ref. 42, an additional dynamical variable s_α is associated to each $S_\alpha(\{\mathbf{R}_I\})$. The extended system is described by the Lagrangian

$$L = L_o + \sum_\alpha \frac{1}{2} M_\alpha \dot{s}_\alpha^2 - \sum_\alpha \frac{1}{2} k_\alpha \{S_\alpha(\{\mathbf{R}_I\}) - s_\alpha\}^2 - V[t, \{s_\alpha\}], \quad (1)$$

where L_o is the Car-Parrinello Lagrangian,³⁴ the second term is the fictitious kinetic energy of the s_α 's, and the third term is a harmonic potential that restrains the value of the collective coordinates $S_\alpha(\{\mathbf{R}_I\})$ to the corresponding dynamical collective variables s_α . $V(t, \{s_\alpha\})$ in Eq. (1) is the history-dependent potential, which is constructed by the accumulation of Gaussians, centered at the positions of the $\{s_\alpha\}$ already visited along the trajectory. The potential discourages the system from remaining in the region already visited and pushes it over the lowest energy barrier toward a new equilibrium basin. We have studied the migration of one oxygen ion toward a nearest-neighbor vacancy using the two collective variables S_1 and S_2 sketched in Fig. 2, namely the distance between the migrating oxygen ion and a Zr^{4+} ion belonging either to the starting (S_1) or the arrival (S_2) tetrahedral cage.

The *ab initio* metadynamics simulations have been performed in the framework of local-density approximation density-functional theory (LDA-DFT) with Goedecker-type pseudopotentials⁴³ and the mixed Gaussian/plane waves basis set implemented in the code QUICKSTEP,^{44–46} due to its lower computational cost compared to CPMD. Double-zeta-valence Gaussian basis sets for Y, Zr, Sc, and double-zeta-valence plus polarization for oxygen have been used. A kinetic cutoff of 260 Ry has been used for plane-wave ex-

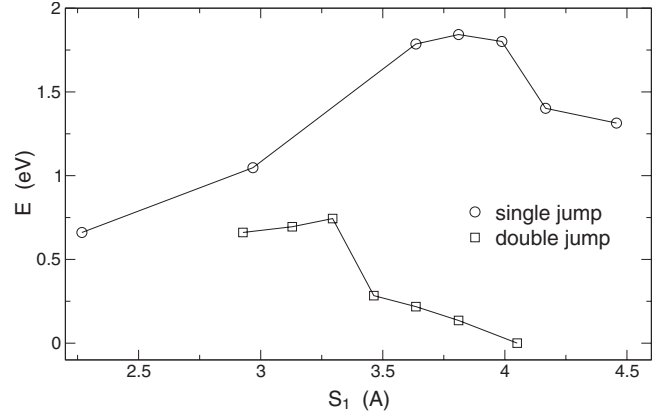


FIG. 3. Potential energy profile for a single- and a double-vacancy jump (see text). The energies are obtained by constrained geometry relaxation at fixed values of the reaction coordinate S_1 (Fig. 2) along the diffusion path.

pansion of the electronic density. The equations of motion are integrated by velocity Verlet with time step of 1.5 fs. The parameters of the Lagrangian [Eq. (1)] have been chosen as $k_\alpha=0.2$ a.u., $M_\alpha=50$ a.m.u.. We have used isotropic Gaussians functions with height $W=0.003$ a.u., and variance $\sigma=0.5$ a.u.⁴² Ionic temperature at 300 K is enforced by a Nosé-Hoover chain thermostat.^{47,48}

We have selected two diffusion processes from the *ab initio* database of Table I, corresponding to the same initial state and different arrival states (different jump directions for the same vacancy). The first process corresponds to an allowed single jump (type 1 in Fig. 1), the second to a concerted double jump which, as described in Sec. II, is observed because the arrival state for a single jump is unstable (type 4 in Fig. 1). We have indeed observed the vacancy jump after 2 and 1 ps of metadynamics simulation, respectively, for the single and double jump. In agreement with previous *ab initio* works^{16–18} we find that the oxygen migration path is approximately a straight line connecting the centers of the two tetrahedra and crossing the metal-metal edge. Actually, it turned out *a posteriori* that the processes identified in the metadynamic simulations would have been equally seen by using just one of the two collective variables S_1 and S_2 .

Activation energies, neglecting entropic contributions, for the single and concerted double vacancy jumps have been computed by constrained dynamics,⁴⁹ using the CPMD code (cf. Sec. II). The profile of the potential energy barrier is obtained by optimizing the geometry at fixed values of the reaction coordinate S_1 (Fig. 2) along the migration path. Also in the case of the double jump only the reaction coordinate S_1 is constrained in the geometry optimization, the second oxygen jumping spontaneously in a concerted way with the motion of the constrained oxygen. This vacancy-vacancy entanglement indicates that the jump corresponds indeed to type 4 in Fig. 1. In all cases the saddle point is the configuration with the oxygen ion at the center of the Zr-Zr edge, in agreement with previous first-principles calculations.^{16–18} The potential energy profile along the diffusion pathway for the single and the double vacancy jump is reported in Fig. 3.

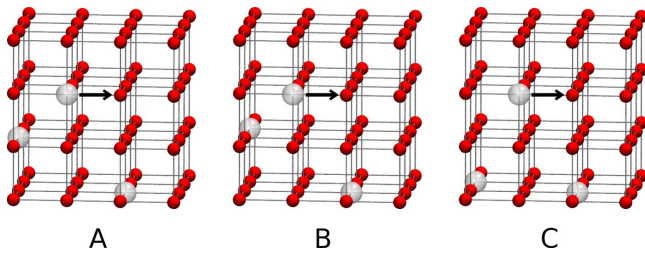


FIG. 4. (Color online) Sketch of the positions of the three vacancies in the three jumps (A, B, and C) considered (cf. Fig. 5 and text). The ideal oxygen sublattice is shown: red spheres are O atoms and big white spheres are O vacancies. The arrow indicates the vacancy jump.

The energy barrier is 0.5–1.2 eV for a single jump, but 0.1–0.7 eV for the double jump, both compatible with the experimental value of $E_a=1.1$ eV.⁵⁰ This result suggests that single and concerted jumps can both contribute to conductivity in YSZ.

To quantify the effect of vacancy-vacancy interaction on diffusion we have calculated, by constrained optimization as described above, the diffusion barrier for three different vacancy configurations, namely for a fixed distribution of Y and fixed position of vacancy V_3 , we let vacancy V_1 perform a jump to a nearest-neighbor site by varying each time the position of V_2 . Vacancies are at least third-nearest neighbor each other and yttrium ions are at least next-nearest neighbor to vacancies. In this way we have obtained the diffusion barrier for a given jump of a vacancy, at fixed yttrium positions, as a function of the position of the other vacancies present in the cell, not involved in the jump itself. A sketch of the relative positions of the three vacancies in the three jumps (A, B, and C) we have considered is given in Fig. 4. The results reported in Fig. 5 show that the potential energy profile for a jump depends significantly on the relative position of the other vacancies, namely the activation barrier and

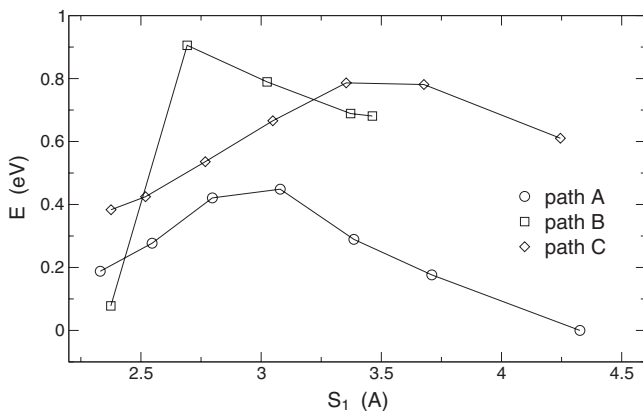


FIG. 5. Potential energy profile for the jump of a vacancy V_1 as a function of the reaction coordinate S_1 in Fig. 2. The three jumps reported (path A, B, and C) differ only for the position of a second vacancy V_2 during the migration of V_1 , while the last vacancy in the simulation cell (V_3) is always in the same position. Vacancies are always at least third-nearest neighbors to each other. Energies are obtained by constrained geometry relaxation at fixed values of the reaction coordinate S_1 (Fig. 2) along the diffusion path.

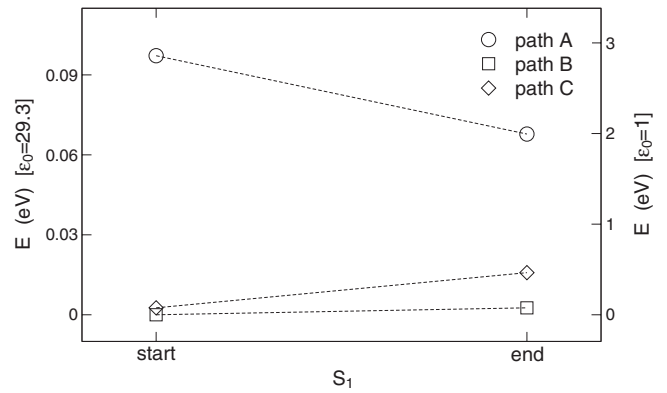


FIG. 6. Variation of the electrostatic energy of the initial and final configurations for three jumps A, B, and C of an oxygen vacancy. The energy is computed by assigning charges +2 and -1 to vacancies and yttrium. The three jumps differ for the relative position of the other vacancies at fixed yttrium distribution (see text). The energies are obtained by the Ewald summation technique for ideal defects position in the fluorite lattice. The energy scale on the left corresponds to electrostatic interactions screened by the experimental dielectric constant [$\epsilon_0=29.3$ (Ref. 51)], which most probably overestimates the screening at the relatively short distance between vacancies (~ 4.4 Å). The energy scale on the right refers to unscreened Coulomb interactions ($\epsilon_0=1$).

energy differences between initial and final states varies in the ranges 0.2–0.8 eV and -0.2–0.6 eV, respectively. This latter variation can be partly related to the difference in electrostatic energy of defects (charge +2 for a vacancy, and -1 for yttrium) between the initial and final configuration of each jump, reported in Fig. 6. However the correlation between Figs. 5 and 6 is just qualitative: the electrostatic energy differences cannot reproduce quantitatively total energy differences, which depend strongly upon the relaxation field around defects as well.

Note that the variation in the jump activation energy due to vacancy-vacancy interactions is comparable with the change induced by the presence of nearest-neighbor yttrium ions, computed theoretically in Ref. 16–18 and summarized in Fig. 7.

Besides Y_2O_3 , other transition metal oxides can stabilize zirconia in the cubic fluorite phase. To assess whether the instability of several vacancy configurations is peculiar to

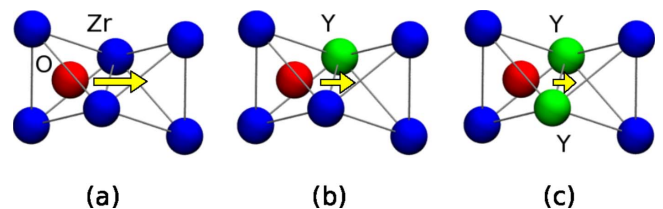


FIG. 7. (Color online) Pathway for oxygen diffusion from the host metal tetrahedron to the nearest-neighbor vacancy site. The different length of the arrows represents the increasing diffusion barrier in passing from (a) Zr-Zr to (b) Zr-Y to (c) Y-Y edges along the path. The activation barriers for processes (a)-(c), calculated from first principles in Refs. 16–18, are 0.5 eV, 0.9–1.3 eV, and 1.3–2.0 eV, respectively.

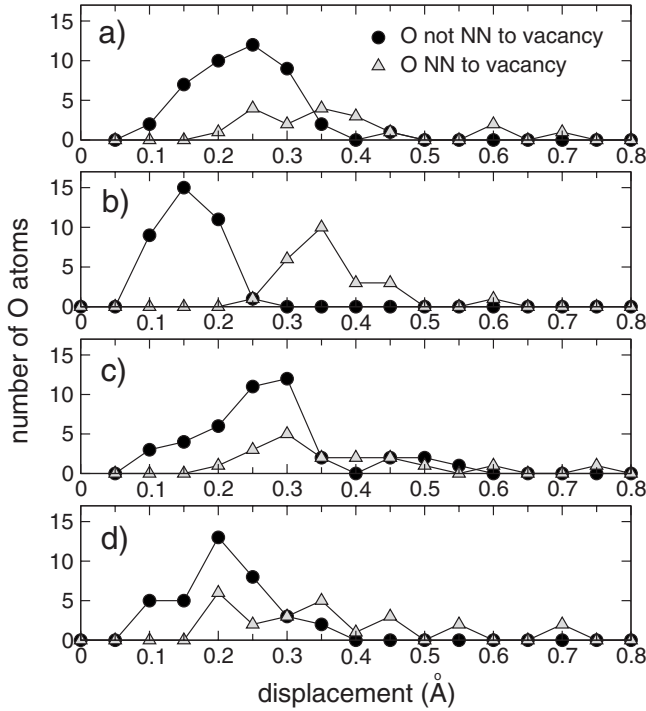


FIG. 8. Distribution of the oxygen atoms displacements with respect to ideal cubic positions in models (93–92 atoms) of cubic zirconia stabilized with (a) 10.3%mol of yttria, (b) 14.3%mol of yttria, (c) 10.3%mol of scandia, and (d) 14.3%mol of scandia. The data on YSZ at 14.3%mol are from our previous work (Ref. 7).

YSZ or it is a common feature of cubic stabilized zirconia, we have considered ScSZ, which shares with YSZ a non-monotonic dependence of ionic conductivity on dopant concentration.¹

Firstly, we have relaxed two models of ScSZ at two different concentration: (i) a model at 10.3% molar content of scandia (three vacancy per cell) with the same distribution of defects of one of the models of YSZ previously discussed and (ii) a model at 14.3% molar content of scandia (four vacancies per cell) with the same distribution of defects of the model of YSZ investigated in our previous work.⁷ Both models are locally stable and display similar relaxation patterns around defects: O atoms relax toward nearest neighbor vacancies along $\langle 100 \rangle$ by $\sim 0.1\text{--}0.6$ Å, while cations relax away from vacancies along $\langle 111 \rangle$ by ~ 0.2 Å. The distributions of oxygen displacements with respect to the ideal fluorite positions are compared for ScSZ and YSZ in Fig. 8.

To assess the effect of vacancy-vacancy interactions on the local stability and diffusion barriers of ScSZ, we have repeated for ScSZ, the zero-temperature calculations reported in Fig. 5 for YSZ (same distribution of defects). The results, reported in Fig. 9, show that vacancy-vacancy interaction has a large effect on the activation energy for diffusion on ScSZ as well, although the energy profiles in Fig. 9 for ScSZ are very different from those reported in Fig. 5 for YSZ. This result further confirms that vacancy-vacancy interaction is produced by the complex relaxation pattern around the vacancy whose details depend on the type of cations as well (the ionic radii of Sc^{3+} and Y^{3+} are 0.8 and 0.9 Å, respectively).

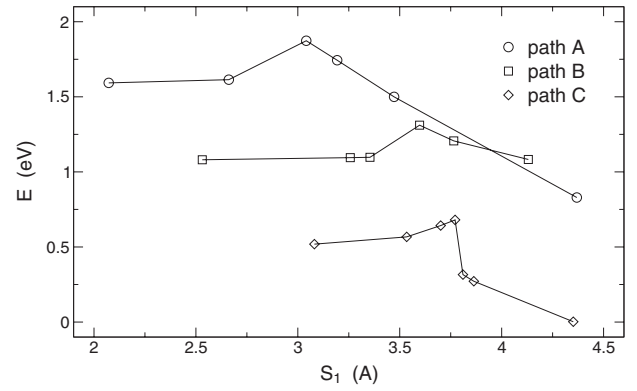


FIG. 9. Potential energy barrier in ScSZ for the jump of a vacancy V_1 as a function of the reaction coordinate S_1 in Fig. 2. The three jumps reported (paths A, B, and C) differ only for the position of a second vacancy V_2 during the migration of V_1 , while the last vacancy in the simulation cell (V_3) is always in the same position. Vacancies are always at least third-nearest neighbors each other. The initial and final configurations are the same of Fig. 5 replacing yttrium with scandium. Energies are obtained by constrained geometry relaxation at fixed values of the reaction coordinate S_1 (Fig. 2) along the diffusion path.

IV. CONCLUSIONS

In summary, we have investigated the role of vacancy-vacancy interactions on oxygen diffusion in YSZ by means of *ab initio* simulations. By studying the stability of 136 defect configurations in 93-atom YSZ supercells, we have found that only half of the configurations are locally stable, the other half reaching a stable state via barrierless vacancy migrations. The exclusion of a large fraction of vacancies configurations can have a sizable effect on the bulk ionic conductivity of YSZ by reducing available diffusion pathways. We remark that we are speaking about configurations in which vacancies are always at least third-nearest neighbor each other. We have discarded the occurrence of important finite-size effects in the *ab initio* 93-atom cell by performing benchmarks on a larger 744-atom cell with empirical two-body interactions.

Investigating the oxygen migration pathways at room temperature by *ab initio* metadynamics, we have found that both single-vacancy and concerted multiple-vacancy jumps occur in YSZ, the concerted ones being the outcome of an attempted jump of a single vacancy toward an unstable final state. Moreover, for a given single-vacancy jump we observed a strong dependence of the activation energy on the relative position of other vacancies, due to medium-range elastic interactions between vacancies mediated by the extended relaxation pattern. This behavior is not peculiar of YSZ but it is reproduced also in scandia-stabilized zirconia. Failed jumps due to instabilities of the arrival configuration introduce deviations from random hopping, which are usually considered responsible for the power-law behavior of frequency-dependent conductivity observed in several solid electrolytes.⁵² Whether the failed (reflected forward-backward) jumps and concerted double jumps found here might be responsible for the power-law conductivity observed in YSZ⁵³ remains to be seen.

So far we have not been able to model the defect-defect interactions responsible for the instability of so many configurations with effective two-body interactions, depending only on the relative positions of yttrium and vacancies on the ideal fluorite lattice, even when a large database of classical simulations is used. Apparently, the elastic interaction cannot be described in simple terms, like the distance between vacancies themselves, but it appears as a complicated many-body problem. Nevertheless our results demonstrate that the relative position of vacancies beyond third-nearest neighbors affect the energy barrier for oxygen diffusion in YSZ. This is

in contrast with the existing models of the conductivity of YSZ, which overlook vacancy-vacancy interaction.

In conclusions, our results point to the need of improving existing lattice models of vacancy diffusion in stabilized zirconia by including vacancy-vacancy interactions in order to better reproduce experimental data on ionic conductivity.

ACKNOWLEDGMENT

This work is partially supported by Cineca through the CNISM-CNR-INFN Parallel Computing Initiative.

- ¹B. C. H. Steele, *J. Power Sources* **49**, 1 (1994).
- ²A. Kivist, *Physics of Electrolytes* (Academic, New York, 1972), Vol. 1.
- ³D. Y. Wang, D. S. Park, J. Griffith, and A. S. Nowick, *Solid State Ionics* **2**, 95 (1981).
- ⁴M. O. Zacate, L. Minervini, D. J. Bradfield, R. W. Grimes, and K. E. Sickafus, *Solid State Ionics* **128**, 243 (2000).
- ⁵M. S. Khan, M. S. Islam, and D. R. Bates, *J. Mater. Chem.* **8**, 2299 (1998).
- ⁶R. E. W. Casselton, *Phys. Status Solidi A* **2**, 571 (1970).
- ⁷G. Stapper, M. Bernasconi, N. Nicoloso, and M. Parrinello, *Phys. Rev. B* **59**, 797 (1999).
- ⁸B. W. Veal, A. G. McKale, A. P. Paulinkas, S. J. Rothman, and L. J. Nowicki, *Physica B (Amsterdam)* **150**, 234 (1988).
- ⁹C. R. A. Catlow, A. V. Chadwick, G. N. Greaves, and L. M. Moroney, *J. Am. Ceram. Soc.* **69**, 272 (1986).
- ¹⁰D. Komyoji, A. Yoshiasa, T. Moriga, S. Emura, F. Kanamaru, and K. Koto, *Solid State Ionics* **50**, 291 (1992).
- ¹¹P. Li, I. Wei Chen, and J. E. Penner-Hahn, *Phys. Rev. B* **48**, 10063 (1993).
- ¹²K. Kawata, H. Maekawa, T. Nemoto, and T. Yamamura, *Solid State Ionics* **177**, 1687 (2006).
- ¹³F. Shimojo and H. Okazaki, *J. Phys. Soc. Jpn.* **61**, 4106 (1992).
- ¹⁴M. Martin, *J. Electroceram.* **17**, 765 (2006).
- ¹⁵M. Meyer, N. Nicoloso, and V. Jaenisch, *Phys. Rev. B* **56**, 5961 (1997).
- ¹⁶R. Krishnamurthy, D. J. Srolovitz, K. N. Kudin, and R. Car, *J. Am. Ceram. Soc.* **88**, 2143 (2005).
- ¹⁷R. Krishnamurthy, Y.-G. Yoon, D. J. Srolovitz, and R. Car, *J. Am. Ceram. Soc.* **87**, 1821 (2004).
- ¹⁸R. Pornprasertsuk, P. Ramanarayanan, C. B. Musgrave, and F. B. Prinz, *J. Appl. Phys.* **98**, 103513 (2005).
- ¹⁹R. Devanathan, W. J. Weber, S. C. Singhal, and J. D. Gale, *Solid State Ionics* **177**, 1251 (2006).
- ²⁰J. P. Goff, W. Hayes, S. Hull, M. T. Hutchings, and K. N. Clausen, *Phys. Rev. B* **59**, 14202 (1999).
- ²¹A. Bogicevic and C. Wolverton, *Phys. Rev. B* **67**, 024106 (2003).
- ²²A. Bogicevic, C. Wolverton, G. M. Crosbie, and E. B. Stechel, *Phys. Rev. B* **64**, 014106 (2001).
- ²³S. Ostanin, A. J. Craven, D. W. McComb, D. Vlachos, A. Alavi, A. T. Paxton, and M. W. Finnis, *Phys. Rev. B* **65**, 224109 (2002).
- ²⁴C. B. Azzoni and A. Paleari, *Phys. Rev. B* **44**, 6858 (1991).
- ²⁵V. M. Orera, R. I. Merino, Y. Chen, R. Cases, and P. J. Alonso, *Phys. Rev. B* **42**, 9782 (1990).
- ²⁶F. Pietrucci, M. Bernasconi, C. Di Valentin, F. Mauri, and C. J. Pickard, *Phys. Rev. B* **73**, 134112 (2006).
- ²⁷J. P. Perdew and A. Zunger, *Phys. Rev. B* **23**, 5048 (1981).
- ²⁸D. Vanderbilt, *Phys. Rev. B* **41**, 7892 (1990).
- ²⁹N. Troullier and J. L. Martins, *Phys. Rev. B* **43**, 1993 (1991).
- ³⁰CPMD, Copyright Ibm corp. 1990–2005, copyright MPI für festkörperforschung Stuttgart 1997–2001, <http://www.cpmd.org>
- ³¹C. Pascual and P. Durán, *J. Am. Ceram. Soc.* **66**, 23 (1983).
- ³²F. Tietz, W. Fischer, T. Hauber, and G. Mariotto, *Solid State Ionics* **100**, 289 (1997).
- ³³G. Ballabio, M. Bernasconi, F. Pietrucci, and S. Serra, *Phys. Rev. B* **70**, 075417 (2004).
- ³⁴R. Car and M. Parrinello, *Phys. Rev. Lett.* **55**, 2471 (1985).
- ³⁵W. H. Press, S. A. Teukolsky, W. T. Vetterling, and B. P. Flannery, *Numerical Recipes in C/Fortran77/Fortran90* (Cambridge University Press, Cambridge, England, 1992).
- ³⁶G. Pacchioni, *J. Chem. Phys.* **128**, 182505 (2008).
- ³⁷H. W. Brinkman, W. J. Briels, and H. Verweij, *Chem. Phys. Lett.* **247**, 386 (1995).
- ³⁸M. Fevre, A. Finel, and R. Caudron, *Phys. Rev. B* **72**, 104117 (2005).
- ³⁹M. Fevre, A. Finel, R. Caudron, and R. Mevrel, *Phys. Rev. B* **72**, 104118 (2005).
- ⁴⁰A. Laio, A. Rodriguez-Forteza, F. L. Gervasio, M. Ceccarelli, and M. Parrinello, *J. Phys. Chem. B* **109**, 6714 (2005).
- ⁴¹A. Laio and M. Parrinello, *Proc. Natl. Acad. Sci. U.S.A.* **99**, 12562 (2002).
- ⁴²M. Iannuzzi, A. Laio, and M. Parrinello, *Phys. Rev. Lett.* **90**, 238302 (2003).
- ⁴³S. Goedecker, M. Teter, and J. Hutter, *Phys. Rev. B* **54**, 1703 (1996).
- ⁴⁴CP2K, released under GPL license, freely available at <http://cp2k.berlios.de>.
- ⁴⁵G. Lippert, J. Hutter, and M. Parrinello, *Theor. Chem. Acc.* **103**, 124 (1999).
- ⁴⁶J. VandeVondele, M. Krack, F. Mohamed, M. Parrinello, T. Chassaing, and J. Hutter, *Comput. Phys. Commun.* **167**, 103 (2005).
- ⁴⁷S. Nosé, *J. Chem. Phys.* **81**, 511 (1984).
- ⁴⁸W. G. Hoover, *Phys. Rev. A* **31**, 1695 (1985).
- ⁴⁹M. Sprik and G. Ciccotti, *J. Chem. Phys.* **109**, 7737 (1998).
- ⁵⁰I. R. Gibson and J. T. S. Irvine, *J. Mater. Chem.* **6**, 895 (1996).
- ⁵¹A. Dwivedi and A. N. Cormack, *Philos. Mag. A* **61**, 1 (1990).
- ⁵²K. Funke, *Prog. Solid State Chem.* **22**, 111 (1993).
- ⁵³C. Leon, M. L. Lucia, and J. Santamaria, *Phys. Rev. B* **55**, 882 (1997).